Journal of Materials Chemistry B

ROYAL SOCIETY OF CHEMISTRY

PAPER

View Article Online
View Journal | View Issue

Cite this: J. Mater. Chem. B, 2025, 13, 6402

Construction and cytotoxicity evaluation of peptide nanocarriers based on coiled-coil structures with a cyclic β-amino acid at the knob-into-hole interaction site†

Monika Szefczyk,[a]* Natalia Szulc,[b] Dominika Bystranowska,[c] Anna Szczepańska,[a] Juan Lizandra Pérez,[a] Anita Dudek,[b] Aleksandra Pawlak,[d] Andrzej Ożyhar[c] and Łukasz Berlicki[a]

Received 1st April 2025,
Accepted 6th May 2025

DOI: 10.1039/d5tb00752f

rsc.li/materials-b

Peptides are highly attractive as nanocarriers for drug delivery and other biomedical applications due to their unique combination of biocompatibility, efficacy, safety, and versatility—qualities that are difficult to achieve with other nanocarrier types. Particularly promising in this context are peptide foldamers containing non-canonical residues, which can yield nanostructures with diverse physicochemical properties. Additionally, the introduction of non-proteinogenic amino acids into the sequence enhances conformational stability and resistance to proteolysis, critical features for bioapplications. In this article, we report the development of novel foldameric bundles based on a coiled-coil structure incorporating *trans*-(1*S*,2*S*)-2-aminocyclopentanecarboxylic acid (*trans*-ACPC) at the key interacting site. We also provide both theoretical and experimental analyses of how this cyclic β-residue affects the thermodynamic and proteolytic stability, oligomerization state, and encapsulation properties of the resulting foldamers compared to standard coiled-coils. Additionally, we assessed the cytotoxicity of these foldamers using the MTT assay on 3T3 cells. The results demonstrate that neither the foldamers nor *trans*-ACPC exhibit toxic effects on the 3T3 cell line, highlighting their potential as safe and effective nanocarriers.

Introduction

Many drug candidates fail to progress through the various stages of preclinical and clinical studies due to a number of reasons, including but not limited to, low solubility, aggregation, high cytotoxicity, poor pharmacokinetic rate, and inefficient site-specific targeting.[1,2] Pharmaceutical research is simultaneously focused on increasing drug stability, enhancing bioavailability, improving organ targeting, maximizing therapeutic efficacy, and minimizing off-target accumulation within the body.[3,4] In this context, drug delivery systems (DDSs) based on synthetic stimuli-responsive polymers are widely studied.[5–8] Nanocarriers, in particular, offer several advantages over traditional drug therapies, as their size, charge, and surface properties can be more easily customized to regulate uptake, biodistribution, targeting, and elimination.[9–11] Various types of nanocarriers have been developed for drug delivery, including liposomes,[12] solid lipid nanoparticles,[13] chitosan,[14] dendrimers,[15] carbon nanotubes,[16] and gold nanoparticles,[17] among others. Peptides have already demonstrated their potential as excellent candidates for bioapplications owing to their exceptional biocompatibility, diverse chemical properties, and structural variety.[18–20] Also as nanocarriers, peptides have gained significant attention due to several unique properties that offer advantages over other compounds, such as versatility in design, targeting specificity, enhanced cellular uptake, ability to overcome biological barriers, low immunogenicity, ease of synthesis and modification.[21–24] However, the use of peptides as drug delivery systems has been significantly hindered by challenges such as variable solubility, low systemic stability, negligible activity

[a] Department of Bioorganic Chemistry, Faculty of Chemistry, Wrocław University of Science and Technology, Wybrzeże Wyspiańskiego 27, 50-370 Wrocław, Poland. E-mail: monika.szefczyk@pwr.edu.pl
[b] Department of Physics and Biophysics, Faculty of Biotechnology and Food Sciences, Wrocław University of Environmental and Life Sciences, Norwida 25, 50-375, Wrocław, Poland
[c] Department of Biochemistry, Molecular Biology and Biotechnology, Faculty of Chemistry, Wrocław University of Science and Technology, Wybrzeże Wyspiańskiego 27, 50-370 Wrocław, Poland
[d] Department of Pharmacology and Toxicology, Faculty of Veterinary Medicine, Wrocław University of Environmental and Life Sciences, Norwida 31, 50-375, Wrocław, Poland

† Electronic supplementary information (ESI) available: Additional figures and tables are available in PDF format *via* the Internet. See DOI: https://doi.org/10.1039/d5tb00752f

upon oral administration, and a short half-life caused by high degradation induced by proteases.[25] Therefore, it is necessary to develop a new generation of peptide-based nanocarriers to overcome these limitations.

Thanks to years of study, along with recently developed theoretical prediction and design models, the sequence–structure relationship in proteins and peptides has been decoded to a large extent, though not fully understood. The best proof of this lies in coiled-coil (CC) peptides.[26,27] In the CC sequence, seven-residue patterns of hydrophobic and polar residues repeat, directing the folding and assembly of amphipathic helices into a superhelix. Surprisingly, these straightforward rules enable the creation of diverse bundles with different oligomerization states and topologies.[28,29] Moreover, CC proved to have structural tolerance, *i.e.*, for the nonheptad sequence inserts[30] or the introduction of unnatural amino acids into the sequence.[31–33] In particular, the use of cyclic β-residues ensures control of the shape of the peptide, leading to distinctly different secondary structural motifs.[34] It also leads to the formation of well-defined three-dimensional structures in solutions (so-called foldamers), and improves their conformational stability and resistance to enzymatic degradation.[35,36] Foldamers, in particular, have exhibited the remarkable ability to self-organize into well-defined higher-order structures with unique characteristics.[37,38] However, there is still much to learn about sequence-to-structure relationships as a means to improve the *de novo* design of foldamers intended for specific applications, such as stimuli-responsive drug delivery systems.[39,40] Especially foldameric bundles, which form tubular architectures with an empty cavity inside, are one of the most promising, in terms of encapsulation and drug delivery, among several higher-order structures formed by peptides,[41–43] and some preliminary studies with model ligands have already been published.[44,45] In this article, we present novel coiled-coil-based bundles with the *trans*-(1*S*,2*S*)-2-aminocyclopentanecarboxylic acid (*trans*-ACPC) at the key interacting *a* site. To the best of our knowledge, no such bundles containing a cyclic beta-amino acid involved in the knob-into-hole interactions in CCs have been described so far. Furthermore, we investigated the influence of the cyclic β-residue on the thermodynamic stability and oligomerization state, and the propensity for encapsulation of the obtained foldameric bundles compared to model CCs. Our results clearly demonstrate that the incorporation of the *trans*-ACPC moiety facilitates the precise tuning of the physicochemical properties of CC peptides. This modification offers the potential to customize these peptides for various ligands and delivery strategies, while simultaneously mitigating common challenges associated with peptide nanocarriers, such as inconsistent solubility, limited conformational stability, and heightened susceptibility to proteolysis.

Experimental section

Peptide synthesis

All commercially available reagents and solvents were purchased from Sigma-Aldrich or Merck and used without further purification. Fmoc-*trans*-(1*S*,2*S*)-2-aminocyclopentanecarboxylic acid (*trans*-ACPC) was purchased from Synnovator, Inc. Peptides were synthesized with an automated solid-phase peptide synthesizer (Liberty Blue, CEM) using rink amide AM resin (loading: 0.59 mmol g^{-1}). Fmoc deprotection was performed using 20% piperidine in dimethylformamide (DMF) for 1 min at 90 °C. A double-coupling procedure was achieved with 0.5 M solution of *N,N′*-diisopropylcarbodiimide (DIC) and 0.5 M solution of Oxyma Pure Novabiochem® (1 : 1) in DMF for 4 min at 90 °C. Acetylation reaction was performed using DMF/*N,N*-diisopropylethylamine (DIPEA)/acetic anhydride (80 : 15 : 5) mixture at room temp. Cleavage of the peptides from the resin was accomplished with the mixture of trifluoroacetic acid (TFA)/triisopropylsilane (TIS)/H_2O (95 : 2.5 : 2.5) after 2.5 h of shaking. The crude peptide was precipitated with ice-cold Et_2O and centrifuged (8000 rpm, 15 min, 2 °C). Peptides were purified using preparative high-performance liquid chromatography (Knauer AZURA ASM 2.1 L) with a C18 column (Hypersil Gold 12 μm, 250 × 20 mm) with water/acetonitrile (0.05% TFA) eluent system.

Analytical high-performance liquid chromatography (HPLC)

Analytical HPLC was performed using a C18 column (ReproSil Saphir 100 Å, 5.0 μm, 4.6 × 150 mm) on Shimadzu system with detection wavelength at 222 nm. Program (eluent A: 0.05% TFA in H_2O, eluent B: 0.05% TFA in acetonitrile, flow 0.5 mL min^{-1}): A: t = 0 min, 90% A; t = 25 or 30 min, 10% A.

Mass spectrometry (MS)

Mass spectra were recorded using a WATERS LCT Premier XE high-resolution mass spectrometer with an electrospray ionization and time-of-flight (TOF) detector.

Circular dichroism (CD)

CD spectra were recorded on JASCO J-815 at 20 °C between 250 and 190 nm with the following parameters: 0.2 nm resolution, 1.0 nm bandwidth, 20 mdeg sensitivity, 0.25 s response, 50 nm min^{-1} scanning speed, 5 scans, 0.1 cm cuvette path length. Typically, the samples were prepared by dilution of peptides stock solution in phosphate buffer (PB, 0.05 M, pH = 7) to obtain peptide concentration of 150 μM (~0.5 mg mL^{-1}). The CD intensity is given as mean residue ellipticity (θ [deg × cm^2 × $dmol^{-1}$]) calculated using the following equation:

$$\theta = \frac{M\theta_{\mathrm{MRE}}}{10c\,\mathrm{ln}}$$

θ = mean residue ellipticity (deg × cm^2 × $dmol^{-1}$); θ_{MRE} = ellipticity (deg × cm^2 × $dmol^{-1}$); c = concentration (mg mL^{-1}); l = path length (cm); n = number of residues.

Temperature denaturation measurements using CD

To examine the thermal unfolding of the peptides, stock solutions were diluted to 0.2 mM and measurement at 208 nm in: (1) water pH = 7 and (2) 3 M guanidinium chloride (GuHCl) were performed. The temperature was increased from 4 to 96 °C in increments of 2 °C. Ellipticity measurements were recorded

with 1-mm path length cuvette, others parameters remained unchanged.

Sedimentation-velocity analytical ultracentrifugation (SV-AUC)

SV-AUC experiments were performed on a Beckman Coulter Proteome Lab XL-I ultracentrifuge (software version 6.0, Beckman Coulter Inc.) equipped with an An-60Ti rotor. The concentrations of the peptides were 50 μM, 80 μM and 100 μM. The samples were suspended in PB buffer either supplemented or not with 50 μM, 100 μM or 500 μM 1,6-diphenyl-1,3,5-hexatriene (DPH). In all the experiments where DPH was added, the concentration of the peptide was 50 μM. Analyses were done at 20 °C and 50 000 rpm using a step size of 0.003 cm, a delay time of 0 s. Parameters obtained with SEDNTRP[46] were as follows: peptide partial specific volumes (0.78033, 0.77647, 0.77473, 0.77327, 0.76815, 0.76669 mL g^{-1} for **KSL**, **KSX**, **QAL**, **QAX**, **QGL**, **QGX**, respectively), buffer density (1.0056 g mL^{-1}) and buffer viscosity (1.0199 mPa × s). Partial specific volumes of the peptides were estimated and corrected for the presence of *trans*-ACPC, N-terminal acetyl, and C-terminal amine moieties using published molar increment values of chemical groups.[47] Time-corrected data[48] were analyzed with SEDFIT software (version 16.1c) using the built-in continuous sedimentation coefficient distribution model, *c*(s). Maximum-entropy regularization of the *c*(s) models was set to a confidence level of 0.68.[49,50]

Ligand binding studies

Ligand binding experiments with 1,6-diphenyl-1,3,5-hexatriene (DPH) were carried out in a 96-well BRANDplate® on a CLARIOstar Plus, BMG LABTECH, at 25 °C for 48 hours. Excitation wavelength of 350 nm and emission wavelength of 450 nm were used. 1 mM stock solution of DPH in PB (5% of DMSO) and 1 mM stock solution of peptides in PB (pH = 7) were used. The experiments were carried out in the concentration range of 5–500 μM. Either the total 500 μM concentration of ligand or peptide was kept constant. The plate was left for 2 h equilibrium before the measurement.

Proteolytic studies

The proteolytic studies were conducted on **KSL** and **KSX** in the presence of α-chymotrypsin (1 : 100 w/w) in 100 mM Tris–HCl buffer (pH = 8.0). The samples were incubated at 25 °C for 2 h before the assay. The proteolytic degradation was monitored by analytical RP-HPLC every 24 hours. Program (eluent *A*: 0.05% TFA in H_2O, eluent *B*: 0.05% TFA in acetonitrile, flow 0.5 mL min^{-1}): *A*: *t* = 0 min, 90% *A*; *t* = 15 min, 10% A.

Cell culture

The study involved the 3T3-NIH cell line. Culture media DMEM-high glucose (Dulbecco's Modified Eagle's Medium, Sigma-Aldrich, St. Louis, MO, USA) was used, supplemented with 10% FBS (Gibco, Grand Island, NY, USA), 1% antibiotic (streptomycin/penicillin, 10.000 μg mL^{-1}, 100 units per mL, Gibco), 1% of L-glutamine (Sigma Aldrich, Steinheim, Germany). Cells were cultivated at 37 °C in a humidified atmosphere containing 5% CO_2 and harvested or passaged by trypsin (0.025% trypsin and 0.02% EDTA; Sigma-Aldrich).

MTT assay

The cytotoxicity assay was performed using the MTT test after 24 and 48 hours of treatment. The cells (6667 cells per 100 μL) were seeded in 96-well plates (NUNC, Denmark) in three replicates and four repetitions for each parameter and incubated at 37 °C for 24 and 48 hours. Peptide nanocarriers were dissolved in Milli-Q® (Merck & Co. Inc., USA) water (pH = 7.0) and vortexed for one minute (stock solution: 1 mg mL^{-1}, approximately 300 μM, depending on the sequence). Then, the stock solution of the given peptide was diluted using DMEM-high glucose. The concentration of the tested foldamers ranged from 1, 5, 10, 15, 25, 50, 75, and 100 μM. Meanwhile, the introduced *trans*-ACPC was dissolved in 1 M HCl (pH ∼0) and vortexed for one minute, followed by the addition of 1 M NaOH (pH ∼14) and another minute of vortexing. The final pH of the solution was approximately 7.1 (stock solution: 1000 μM) and was further diluted with culture media to concentrations of 1, 5, 10, 15, and 25 to 200 μM in 25 μM increments. After incubation for 24 and 48 hours, 10 μL of 3-(4,5-dimethylthiazol-2-yl)-2,5-diphenyltetrazolium bromide (MTT) solution was added to each well, followed by a 4-hour incubation. Then, 40 μL of lysis buffer was added. The optical density (OD) of the formazan formed from MTT was measured after 24 hours using a spectrophotometric microplate reader (Spark, Tecan, Männedorf, Switzerland) at a reference wavelength of 570 nm. The results were analyzed as a percentage of viable cells compared to untreated control cells.

Statistical analysis

Statistical analysis was conducted using Python (version 3.10.0) with the Pandas, NumPy, SciPy, Statsmodels, Seaborn, and Matplotlib libraries. The normality of cell viability data was assessed using the Shapiro-Wilk test, while homogeneity of variances was evaluated using Levene's test. A two-way ANOVA was performed to examine the effects of *trans*-ACPC concentration and incubation time (24 h *vs.* 48 h) on cell viability, followed by Tukey's Honest significant difference (HSD) *post hoc* test to determine specific differences between time points. For groups violating normality assumptions, log transformation was applied to improve data distribution. Statistical significance was set at $p \leq 0.05$, and all results were visualized using Seaborn and Matplotlib, with bar plots including error bars (standard deviation) and annotations where applicable. Whereas, for peptide nanocarriers, a three-way ANOVA was conducted to evaluate the effects of peptide type, peptide concentration, and incubation time (24 h *vs.* 48 h) on cell viability. HSD *post hoc* test was applied to further explore significant differences between specific groups. To ensure the validity of statistical assumptions, Shapiro-Wilk test was used to assess data normality, and Levene's test was performed to evaluate the homogeneity of variances. In cases where the normality assumption was violated, log transformation was applied to improve data distribution. Pairwise comparisons

were conducted between each concentration and the control (0 μM) for each peptide, with significance levels indicated using statannotations in the visualization (Fig. S10, ESI†). A significance threshold of $p \leq 0.05$ was applied for all statistical analyses.

Molecular modelling

Initial models based on crystal structures. The PDB files were processed with Discovery Studio Visualizer (v17.2.0), where the corresponding residues were modified with *trans*-ACPC and then superimposed over the native crystal structure.

KSX: construction based on crystal structures of CC_Hex2 (PDB:4PN9)

QGX: construction based on crystal structures of CC_Type2_(GgLaId)4 (PDB:7BIM)

QAX: construction based on crystal structures of CC_Hept (PDB:4PNA)

Parametrization of DPH

The DPH structure was initially created using Avogadro software. A conformation search was performed within the same program, and the lowest-energy conformation of the ligand was minimized using the GAFF (General Amber Force Field) in Avogadro. A Gaussian input file was then generated for a final energy minimization in Gaussian 16, employing the AM1 level of theory. After minimization, the structure was parametrized using GAFF, and partial charges were calculated with Antechamber using the AM1-BCC method. The final parameter files (DPH.frcmod and DPH.lib) were generated using Parmchk2 and TLeap.

Initial structures

The pdb4amber tool was employed to remove water molecules and hydrogens from the inserted *trans*-ACPC. The cleaned structures were then processed with TLeap (AmberTools21) to generate the topology and initial coordinates files, using the leaprc.mimetic.ff15ipq force field. A preliminary minimization of the structures in a vacuum was conducted to prepare these files for future use.

Docking of DPH

AutoDockTools (ADT) was used to generate the PDBQT files for the DPH ligand and the studied peptides. The peptides were processed according to the ADT protocol, with grid parameters set to ensure the entire channels were included in the docking grid. For the ligand, the Gaussian-minimized structure was used without imposing any torsional degrees of freedom. The generated files were then used in AutoDock Vina, with exhaustiveness set to 100, to produce the 10 lowest-energy binding poses based on the ADV scoring function. The results are summarized in Table S5 and visualized in Fig. S11 in ESI.†

Updated models based on our experimental results

The number of helices forming the coiled-coil homomers has been revised to align with our experimental findings. Size discrepancies may arise due to the origin of the initial models, which were based on X-ray crystallography data. As a result, the bundles formed in solution could vary significantly from these models.

Preparation of the updated structures

The PDB crystal structures, mentioned earlier in this section, were used to adjust the oligomerization states of the theoretical models in accordance with the experimental results. The model construction process followed the same methodology outlined above. The resulting structures are shown in Fig. S12 in ESI.† The possibility of encapsulating two DPH molecules was also considered and summarized in Table S6 and visualized in Fig. S13 (ESI†).

Molecular dynamics

Prior to system preparation for calculations, the SOLVATE program was used on each minimized system to create a solvation shell of 5 Å TIP3P water molecules around the protein, and 8 Gaussians were applied to define the solvent surface. This ensures effective solvation within the protein bundles. The pre-solvated structures were then processed using tleap in AmberTools21, where a truncated octahedron solvent model with 5 Å padding and a proximity of 0.75 Å was implemented, followed by charge neutralization with NaCl. The protein was parameterized using leaprc.mimetic.ff15ipq due to the presence of *trans*-ACPC, and the ligand was defined using the custom parameters DPH.frcmod and dph.lib.

Energy minimization

Energy minimization was performed in four stages, each consisting of 500 steps of steepest descent followed by 9500 steps of conjugate gradient. The coordinates from each minimization step were used in the subsequent stage:

1. Water molecules, ions, and hydrogen atoms were minimized, while all other heavy atoms were restrained with Cartesian forces of 25 kcal mol^{-1}.

2. Side chains were minimized by applying gradient restraints on backbone and ligand atoms, reducing from 25 kcal mol^{-1} to 5 kcal mol^{-1}.

3. The system was minimized with restraints of 1 kcal mol^{-1} on alpha carbons and ligand atoms.

4. The final minimization was performed without restraints on the entire system.

Heat equilibration phase

During the heat equilibration phase, the temperature was gradually increased from 0 to 300 K over 18 ps, followed by an additional 2 ps at 300 K. A 5 kcal mol^{-1} restraint was applied to the backbone and ligand atoms, and Langevin dynamics with a gamma_ln value of 5 ps^{-1} was used for temperature regulation.

Equilibration at constant pressure

NPT equilibration was performed using Langevin dynamics with a gamma_ln of 5 ps^{-1}. The Berendsen barostat was applied to maintain the pressure at 1.01325 bar, with a pressure

relaxation time (tautp) of 1 ps. Backbone restraints were imposed and gradually reduced from 5 kcal mol^{-1} to 1 kcal mol^{-1} over a 1 ns simulation.

Final equilibration

The system was then equilibrated for an additional 2 ns without any restraints. This was followed by a 500 ns production MD simulation using the pmemd.cuda application. The VU Bazis Computational Cluster was utilized for simulations, and trajectory analysis was carried out using cpptraj.

Results

Design

Firstly, we have chosen three coiled-coil peptides from the Protein Data Bank (PDB): **KSL** (PDB ID: 4PN9), **QAL** (PDB ID: 4PNA), and **QGL** (PDB ID: 7BIM) (Table 1), which possess different oligomerization states (hexamer, heptamer, and octamer, respectively). The peptides are characterized by the two distinct *a* + *e* and *d* + *g* hydrophobic interfaces and the electrostatic interactions between the *b* and *c* positions resulting in a $(hpphhph)_n$ repeating pattern (Fig. 1A). Type II interfaces are favorable for the construction of bundles with a high-oligomerization state suitable for encapsulation.[51] The peptides have four heptad repeats with a (*cdefgab*) register to maximize $c_{i-1} \rightarrow b_i$ salt bridges in parallel homomers. The hydrophobic cores of CCs (positions *a* and *d*), which form knob-into-hole interactions between the helices, are usually constructed from aliphatic amino acids rather than other residues.[52,53] The use of cyclic β-amino acids for this purpose seems to be justified by their hydrophobic properties; however, previous attempts to introduce cyclic residues in the key interacting sites of CCs have failed.[54] In our earlier studies, we showed that the *trans*-ACPC residue (Fig. 1B) is well tolerated in the coiled-coil structure[32–34,55] and it can improve its conformational stability against environmental factors (*e.g.*, pH, temperature, proteases) compared to the unmodified counterparts. We also demonstrated that foldamers can possess a strikingly different propensity for encapsulation despite the sequence similarity.[56] To take a closer look at this phenomenon, we designed three α,β-foldamers based on the model CC peptides, namely **KSX**, **QAX**, and **QGX**, where the *trans*-ACPC was introduced in a position *a*, responsible for key hydrophobic interactions (Table 1 and Fig. 1C). 1,6-Diphenyl-1,3,5-hexatriene (DPH, Fig. 1D) was chosen as a model ligand to assess the encapsulation properties of the obtained foldamers, as it is a hydrophobic molecule well suited for the cavities of the designed nanocarriers.

Table 1 Sequences of the studied peptides

Name	Sequence
KSL	Ac-GEIAKSLKEIAKSLKWIAKSLKEIAKSLKG-NH_2
KSX	Ac-GEIAKSXKEIAKSXKWIAKSXKEIAKSXKG-NH_2
QAL	Ac-GEIAQALKEIAKALKEIAWALKEIAQALKG-NH_2
QAX	Ac-GEIAQAXKEIAKAXKEIAWAXKEIAQAXKG-NH_2
QGL	Ac-GEIAQGLKEIAKGLKEIAWGLKEIAQGLKG-NH_2
QGX	Ac-GEIAQGXKEIAKGXKEIAWGXKEIAQGXKG-NH_2

According to the performed molecular modeling, the oligomerization states of the α,β-peptides containing *trans*-ACPC (**KSX**, **QAX**, and **QGX**; Fig. 2B and C) should be the same as for the corresponding model peptides (**KSL**, **QAL**, and **QGL**; Fig. 2A). The docking studies demonstrated that the sizes and shapes of the channels are suitable for the encapsulation of DPH (Fig. 2D and Fig. S11, Table S5, ESI†).

Structural studies

The designed peptides were synthesized using solid-phase peptide synthesis (SPPS) on a fully automated synthesizer, purified using a preparative reverse-phase high-performance liquid chromatography (RP-HPLC), and then subjected to qualitative analysis (Table S1 and Fig. S1, ESI†). Subsequently, we performed structural studies using circular dichroism (CD) and analytical ultracentrifugation (AUC) to verify our sequence design and the modeling based on PDB data. CD spectroscopy (Fig. 3A and Fig. S2, ESI†) indicated that **KSL**, **QAL**, and **QGL** are helical in phosphate buffer solution (C = 0.05 M, pH = 7) at low micromolar concentrations, showing minima at λ = 208 and 222 nm. **KSX**, **QAX**, and **QGX** possess a distinct minimum at approximately 208 nm, characteristic for helical α,β-peptides. Thermal denaturation studies using CD (Fig. S3, ESI†) showed higher conformational stability for peptides containing *trans*-ACPC in the first two groups of peptides (**KSX** *vs.* **KSL** and **QAX** *vs.* **QAL**). However, **QGX** exhibited the lowest conformational stability among all the studied peptides.

On the basis of AUC analysis, we noticed substantial differences in the oligomerization states of the studied peptides, also in comparison to the models deposited in the PDB database. Peptides **KSL** (Fig. 3B) and **QAL** (Fig. S4, ESI†) sedimented with a single narrow peak, and the value of the obtained sedimentation coefficients corresponded exclusively to the mass of either the heptamer or the hexamer (for **KSL** and **QAL**, respectively). **QGL** existed mainly as a hexamer in solution (Fig. S4, ESI†), but a fraction of monomers was detected. Incorporating *trans*-ACPC into the peptide **KSX** (Fig. 3) resulted in the formation of oligomers of higher molecular weight (Table S2, ESI†). In contrast, the oligomerization state of **QAX** remained unchanged (Fig. S4, ESI†). The data obtained for **QGX** (Fig. S4, ESI†) revealed two significant species, one likely related to the monomeric state of the peptide and the second being consistent in size with what is expected for a hexamer.

Differences were observed between the oligomerization states obtained for the theoretical models deposited in the PDB and the results from the SV-AUC measurements (Fig. 2 and Table S2, ESI†). The experimental results showed that **KSL** and **KSX** are heptamers, whereas the PDB-based models assumed hexamers. **QAL** and **QAX** proved to be hexamers in solution and heptamers in modeling data. **QGL** and **QGX** are also hexamers according to SV-AUC results and not octamers as in the models. Moreover, **QGX** possessed a high content of monomeric species, which is in concordance with CD studies showing its lower conformational stability (Table 2).

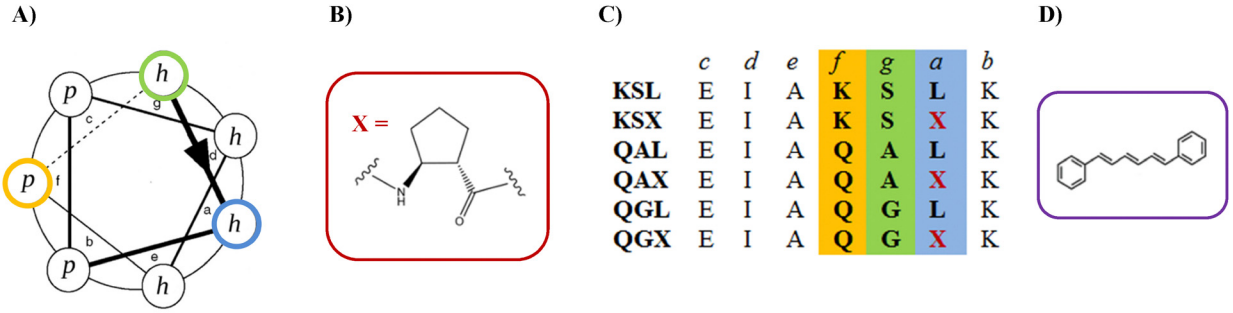

Fig. 1 (A) Helical wheel representing the arrangement of hydrophobic (*h*) and polar (*p*) amino acids in a single helix. (B) The structure of the *trans*-(1*S*,2*S*)-2-aminocyclopentanecarboxylic acid (*trans*-ACPC) residue. (C) $(cdefgab)_4$ register representing $(phhphhp)_n$ pattern with the specified amino acid composition of the studied peptides. (D) The structure of the ligand: 1,6-diphenyl-1,3,5-hexatriene (DPH).

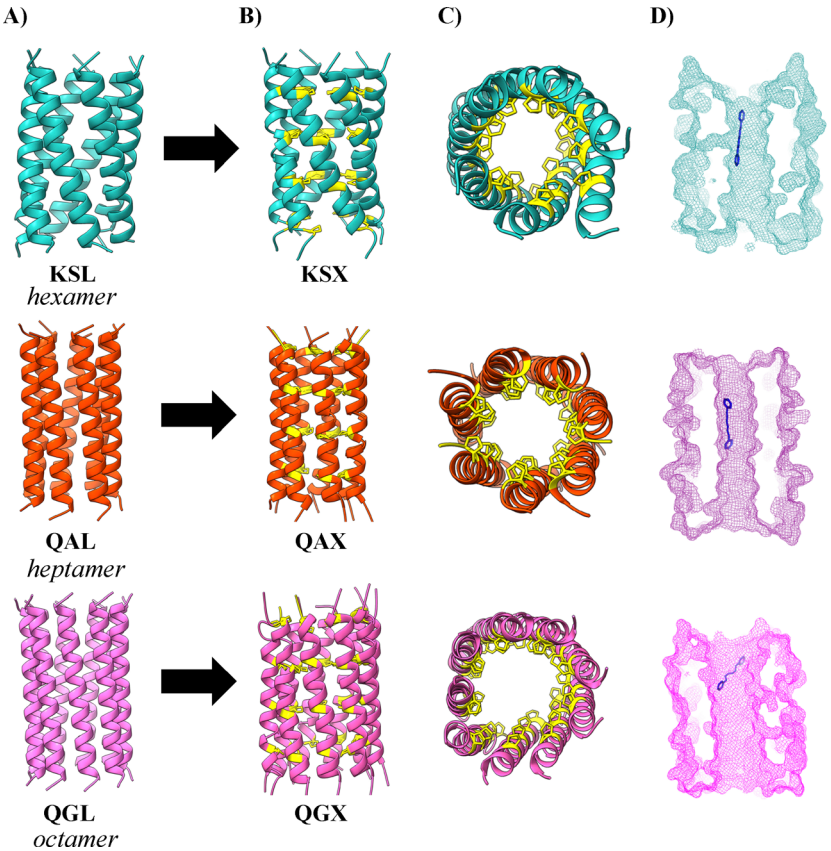

Fig. 2 (A) The crystal structures of the homomeric coiled-coil assemblies (PDB ID: 4PN9 (**KSL**), 4PNA (**QAL**), 7BIM (**QGL**)) in the cartoon representation. (B) Side and (C) top views of the models obtained after inserting *trans*-ACPC (yellow) into the sequence. (D) The mesh cross-sections of *trans*-ACPC-containing peptides are shown with the DPH ligand docked inside, illustrating the size and shape of the channel.

Encapsulation studies

We used 1,6-diphenyl-1,3,5-hexatriene (DPH) as a model ligand to test the capacity of the obtained foldamers for the encapsulation of the hydrophobic molecule. To begin with, 500-ns of unrestrained molecular dynamics (MD) simulations were performed (Fig. 4). During the analysis of the trajectories, no significant differences were observed on the capacity of each peptide to retain DPH. However, **KSX** showed the largest deviation from the starting point, with significant distortion of the channel, which appears to collapse around DPH along the simulation (Fig. S6, ESI†).

Following the modeling, fluorescence studies were performed to experimentally demonstrate the capacity of the coiled-coils to encapsulate DPH. This was possible thanks to the resulting increase in DPH fluorescence after entering the nanocarrier channel, which blocked the free rotation of the rings. Therefore, we compared the ability of each peptide for ligand encapsulation (Fig. 5). The ligand binding studies were

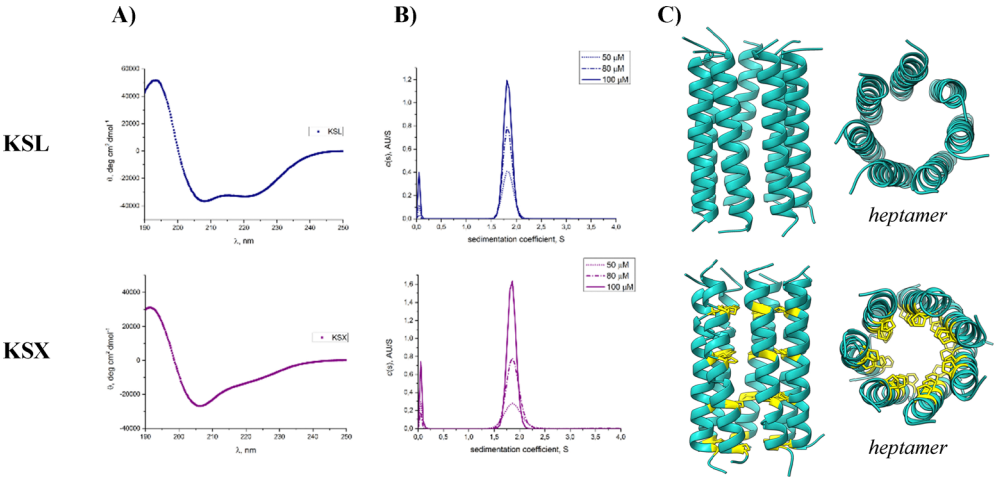

Fig. 3 Representative sample data for **KSL** and **KSX** peptides: (A) CD spectra, (B) SV-AUC sedimentation coefficient distributions, and (C) models based on experimental data. The results for the other peptides are presented in Fig. S4 (ESI†).

Table 2 Comparison of the theoretical and experimental oligomerization states of the studied peptides, as determined by molecular modeling and SV-AUC, respectively

Peptide	Theoretical oligomerization state	Experimental oligomerization state
KSL	Hexamer	Heptamer
KSX	Hexamer	Heptamer
QAL	Heptamer	Hexamer
QAX	Heptamer	Hexamer
QGL	Octamer	Hexamer
QGX	Octamer	Hexamer/monomer

carried out at peptide and ligand concentration ranges of 5–500 μM (Fig. S7, ESI†).

It can be concluded that **KSL** and **KSX** show the highest propensity for ligand encapsulation, whereas **QGX** shows hardly any ability as a nanocarrier. Additionally, SV-AUC studies were carried out in the presence of the different concentrations of DPH (Fig. S8 and Table S3, ESI†). **QAL**, **QAX**, and **QGL** maintained their hexamer oligomerization state in the presence of DPH. **KSL** exhibited both hexameric and heptameric populations, whereas the **QGX** sample preserved a high content of monomers. Interestingly, the **KSX** sample showed an increasing population of smaller oligomers (especially

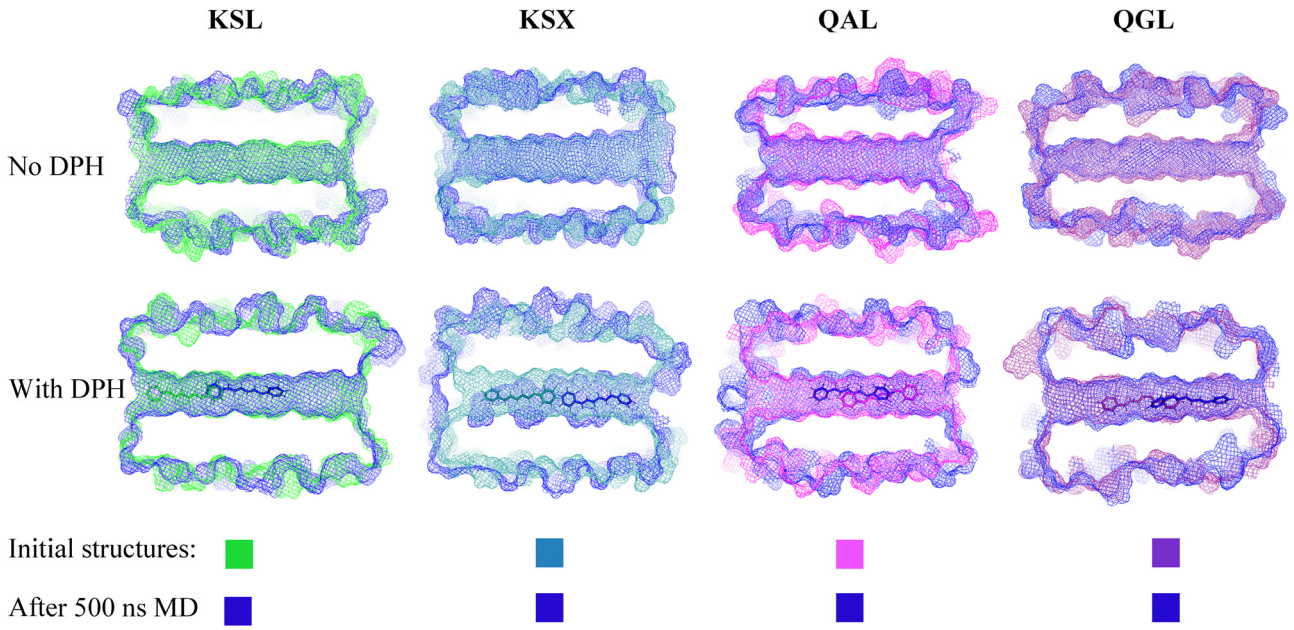

Fig. 4 Results of the 500-ns-long molecular dynamics (MD) simulation for each coiled-coil assembly without (top) and with (bottom) 1,6-diphenyl-1,3,5-hexatriene (DPH, Fig. 1B) ligand docked in the channel. The initial models have been depicted in different colors (green: **KSL**; teal: **KSX**; magenta: **QAL**; purple: **QGL**), while the superimposed navy models correspond to the structure after 500-ns MD in water.

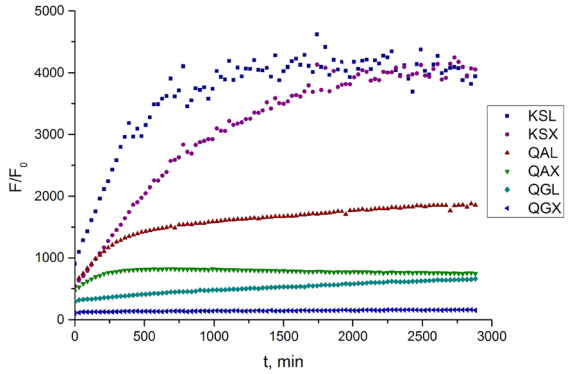

Fig. 5 Fluorescence studies of the DPH encapsulation in the obtained peptides in time. C_{pep} = 500 μM, C_{lig} = 5 μM, pH = 7, t = 48 h, T = 25 °C.

monomers) with an increase in DPH concentration. The molecular dynamics also showed that the **KSX** peptide has a propensity to collapse within the simulation time (Fig. S6, ESI†). Therefore, both AUC and MD suggest that a single helix might separate from a bundle after DPH encapsulation.

Proteolytic studies

Finally, proteolytic stability tests with α-chymotrypsin were performed on the best candidates for nanocarriers, namely **KSL** and **KSX**. The enzymatic degradation was monitored using analytical HPLC for 3 days (Fig. S9, ESI†). The results demonstrated that the *trans*-ACPC-containing peptide **KSX** exhibited increased proteolytic stability (26% degradation) compared to the model peptide **KSL** (93% degradation) (Table S4, ESI†).

Cytotoxicity assay

The MTT assay provides information about mitochondrion activity in cells exposed to various foldamers concentrations (Fig. 6 and 7). Fig. 6 presents the effects of *trans*-ACPC peptide concentration on cell viability at 24 h and 48 h, assessed using the MTT assay, which measures mitochondrial activity as an indicator of cell survival. The results are expressed as the percentage of viable cells relative to the untreated control. Overall, no significant effect of peptide concentration on cell viability was observed (p = 0.5029, Two-Way ANOVA), while time (24 h *vs.* 48 h) had a significant impact (p = 0.0449), indicating potential time-dependent changes in cell response.

The Shapiro–Wilk test confirmed that most groups followed a normal distribution, except for 15 μM (24 h) and 175 μM (24 h), which violated normality assumptions, suggesting the need for data transformation or non-parametric tests. Levene's test (p = 0.9356) confirmed homogeneity of variance, ensuring the reliability of ANOVA results. These findings provide initial insights into the cytocompatibility of *trans*-ACPC, serving as a reference for further studies on peptide-based nanocarriers. In the next step the cytotoxicity of peptide nanocarriers based on coiled-coil structures (Fig. 7). The study examined the effect of different peptide concentrations (1–100 μM) on 3T3-NIH fibroblast cells at 24 and 48 hours of incubation. Overall, cell viability remained above 60% for most peptide concentrations, suggesting low cytotoxicity across the tested conditions. Some peptide variants exhibited a dose-dependent decrease in viability at higher concentrations (≥50 μM), indicating potential cytotoxic effects at elevated doses. Statistical analysis revealed significant differences in cell viability between various peptide concentrations and incubation times, suggesting a complex interaction between peptide type, dose, and exposure duration (Fig. S10, ESI†). Notably, a slight reduction in viability was observed at 48 hours compared to 24 hours, indicating a time-dependent response to peptide exposure. However, for most peptides, cell viability remained relatively stable across time points, with minimal toxic effects at lower concentrations.

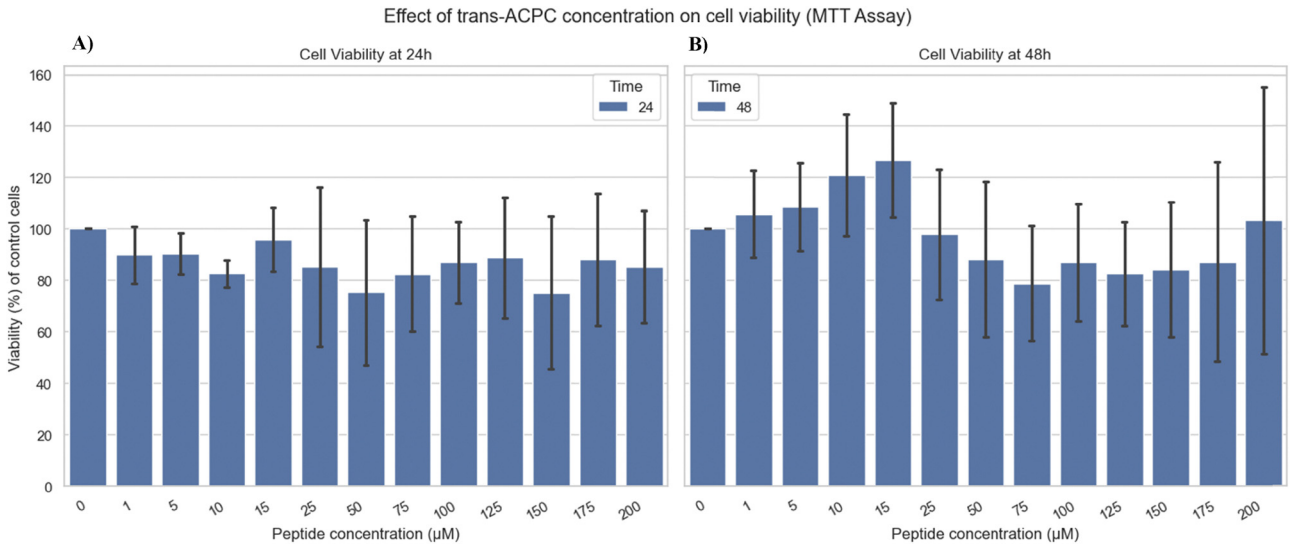

Fig. 6 The effect of *trans*-ACPC concentration on cell viability assessed by MTT assay. (A) Cell viability of 3T3 cells after 24 h of treatment. (B) The cell viability under the same conditions after 48 h. Results are expressed as a percentage of control cell viability. Bars represent mean ± standard deviation ($n \leq 4$).

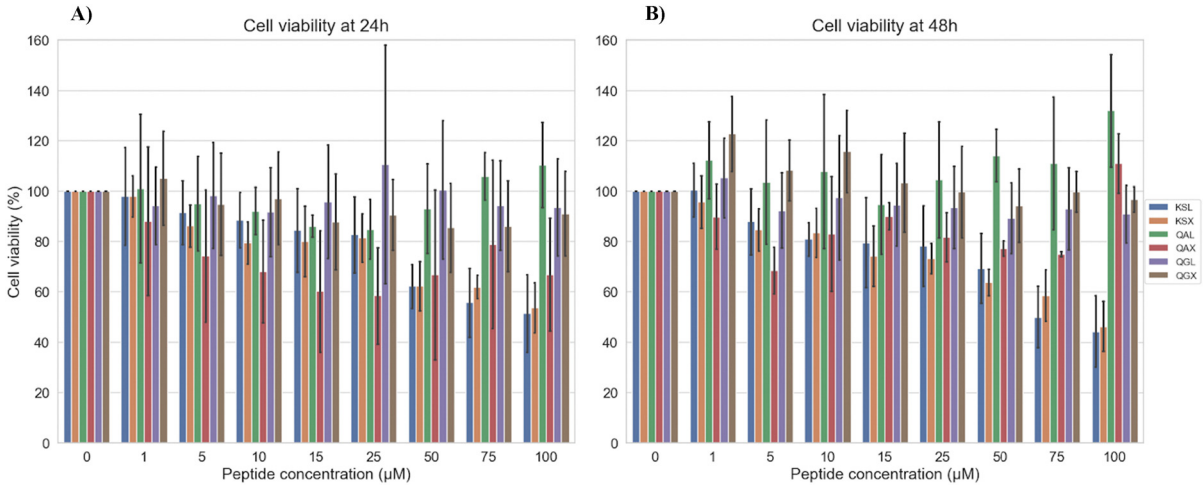

Fig. 7 The effect of peptide nanocarriers based on coiled-coil structures concentration on cell viability assessed by MTT assay. (A) Cell viability of 3T3 cells after 24 h of treatment. (B) The cell viability under the same conditions after 48 h. Results are expressed as a percentage of control cell viability. Bars represent mean ± standard deviation ($n \leq 4$).

Certain peptides, such as **QAX** and **QGX**, showed more pronounced cytotoxic effects at higher concentrations, whereas **KSL** and **KSX** maintained relatively higher viability, suggesting better biocompatibility. The presence of large error bars in some conditions indicates variability in cellular responses, possibly due to biological differences or peptide aggregation at higher concentrations.

Discussion

CD measurements revealed that the model peptides **KSL**, **QAL**, and **QGL** adopt helical structures, while the *trans*-ACPC-containing **KSX**, **QAX**, and **QGX** display characteristics typical of helical α,β-peptides. Additionally, SV-AUC experiments demonstrated the formation of barrels, confirming that *trans*-ACPC is well tolerated within the coiled-coil structure, including in the key knob-into-hole interaction site. Previous attempt to incorporate this cyclic β-residue in the *a* position of coiled-coils was unsuccessful.[54] However, it appears that this was not due to ACPC's inability to form hydrophobic interactions with Ile (or rather Leu), as previously suggested, but rather because successful coiled-coil stabilization also depends on crucial electrostatic interactions and the positioning of other amino acids in the heptad repeats. Interfaces of the Type II pattern $(hpphhph)_n$ proved more favorable than the previously studied Type N $(hpphppp)_n$ not only for constructing barrels with higher oligomerization states but also for facilitating the incorporation of cyclic β-residues in hydrophobic core interactions.

Thermal denaturation studies using CD showed that the presence of *trans*-ACPC in the structure generally enhances the conformational stability of the foldamers compared to their unmodified counterparts, with the exception of **QGX**. This discrepancy is likely due to the high monomer content in **QGX** samples, as indicated by SV-AUC data. Notably, while peptides **QAX** and **QGX** differ only at the *g* position (Ala *vs.* Gly), their oligomerization states and, particularly, their conformational stabilities vary significantly. Alanine, when positioned internally within a helix, is considered one of the most stabilizing residues, whereas glycine—second only to proline—tends to be more destabilizing. Alanine consistently stabilizes the helical conformation relative to glycine, as it buries a larger apolar surface area upon folding and has lower backbone entropy.[57] However, the stabilizing effect of Ala relative to Gly on helix formation is strongly dependent on its specific position in the helix (such as internal *vs.* terminal) and on the surrounding amino acid context.[58]

Moreover, SV-AUC measurements showed that, although the introduction of *trans*-ACPC does not alter the oligomerization state relative to model peptides, discrepancies exist between the oligomerization states obtained from molecular modeling based on PDB data and those observed experimentally. These discrepancies likely arise because PDB models are derived from X-ray crystallography data, while AUC analyses are conducted in solution, providing a setting that more closely resembles the environment of peptides.

According to the *in silico* studies, all peptides show similar capacity to encapsulate and retain DPH. However, the experimental studies showed that both **KSL** and **KSX** possess the highest propensity for DPH encapsulation. This is likely because, as heptamers, they have the largest channel and, therefore, can easily accommodate DPH. However, the optimal number of helices for interactions with DPH seems to be six, as we observed a predominant hexameric population in **KSL** and, even more interestingly, a single helix being pushed out from the heptameric **KSX** after interaction with DPH. As expected, for **QGX**, a high content of monomeric species is not suitable for the ligand encapsulation. The interactions between the barrels and DPH were strong enough to retain DPH inside, as indicated by sustained high fluorescence that tend to plateau after 48 hours. The oligomeric states of the assemblies remained unaffected by the presence of the small molecule, as demonstrated by SV-AUC analysis.

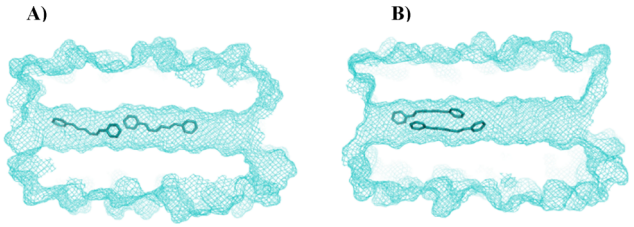

Fig. 8 An alternative docking of two DPH molecules to **KSX**.

KSL and **KSX** exhibit distinct DPH binding kinetics compared to the other peptides. This divergence may stem from the binding of two ligand molecules within the cavity of **KSL** and **KSX**. To investigate further, we conducted molecular modeling from two different initial DPH positions (Fig. 8). In both scenarios, equilibrium was reached with the molecules adopting a parallel arrangement orientation, as shown in Fig. S13 in ESI.†

Moreover, the studied peptides possess similar hydrophobic cores: Ile/Leu for **KSL**, **QAL**, and **QGL**, or Ile/*trans*-ACPC for **KSX**, **QAX**, and **QGX**, which could explain why molecular modeling shows no difference in their theoretical propensity for encapsulation. However, experimental studies exhibited different behavior for each peptide in the presence of the ligand. It can be hypothesized that the residues outside of the hydrophobic core can have a significant influence on the overall ligand-nanocarrier interactions, either facilitating or hindering the encapsulation process.

The results of the MTT assay confirm that peptide-based nanocarriers exhibit low cytotoxicity, with cell viability remaining above 60% for most tested concentrations. The overall stability of cell viability across different peptide concentrations and incubation times suggests that these coiled-coil foldamers are well tolerated by 3T3-NIH fibroblast cells. The peptides **KSL** and **KSX**, in particular, maintained higher biocompatibility, making them promising candidates for nanocarrier applications. These findings indicate that peptide nanocarriers could be effectively utilized for drug delivery systems, offering a balance between biocompatibility and functional stability.

Conclusions

In conclusion, novel foldameric bundles based on the coiled-coil structure with *trans*-ACPC at the key hydrophobic interacting site were obtained. The CD and SV-AUC results indicated that *trans*-ACPC can be well tolerated in the CC structure and does not influence the oligomerization state, while increasing the conformational stability compared to the model peptides. However, we noticed discrepancies of the oligomerization states between the results based on crystal data and those obtained in solution. There is no significant difference between the theoretical encapsulation models of the studied peptides; however, experimental results showed some ligand preferences. As expected, a higher oligomerization state is beneficial for channel entering. Moreover, *trans*-ACPC introduces conformational flexibility into selected nanocarrier structure, affecting its ability to accommodate ligands of certain sizes and shapes. Interestingly, the DPH ligand showed some preferences for interactions with hexameric structures, even by pushing out a helix from the heptamers. The best performance was exhibited by **KSL** and **KSX** peptides, whereas **QGX** proved to be inefficient in DPH encapsulation. Comparison of the experimental results with theoretical studies showed the influence of the peripheral residues on the encapsulation propensity of the scaffolds. Moreover, β-residue-containing peptide **KSX** exhibited increased proteolytic stability compared to the model peptide **KSL**. Our findings show that incorporating the *trans*-ACPC residue allows for adjustment of the physicochemical properties of CC peptides. This modification provides the flexibility to tailor these peptides for different ligands and delivery methods while addressing common issues faced by peptide nanocarriers, such as variable solubility, low conformational stability, and vulnerability to proteolysis. Notably, the MTT assay results showed that the studied peptides have low cytotoxicity, so they represent promising candidates for therapeutic applications.

Abbreviations

CC	Coiled-coil
CD	Circular dichroism
DDS	Drug delivery system
DIC	*N,N′*-diisopropylcarbodiimide
DIPEA	*N,N*-diisopropylethylamine
DMF	Dimethylformamide
DPH	1,6-Diphenyl-1,3,5-hexatriene
GuHCl	Guanidinium chloride
MD	Molecular dynamics
MS	Mass spectrometry
MTT	3-(4,5-dimethylthiazol-2-yl)-2,5-diphenyltetrazolium
OD	Optical density
PB	Phosphate buffer
PDB	Protein Data Bank
RP-HPLC	Reverse phase high-performance liquid chromatography
SPPS	Solid-phase peptide synthesis
SV-AUC	Sedimentation-velocity analytical ultracentrifugation
TFA	Trifluoroacetic acid
TIS	Triisopropylsilane
trans-ACPC	*Trans*-(1*S*,2*S*)-2-aminocyclopentanecarboxylic acid
TOF	Time-of-flight

Data availability

The data supporting this article have been included as part of the ESI.†

Conflicts of interest

Authors declare no potential conflict of interest.

Acknowledgements

The project was co-financed by the Polish National Agency for Academic Exchange, grant no. BPN/BPT/2021/1/00012 (to M. S.).

References

1 J. P. Hughes, S. Rees, S. B. Kalindjian and K. L. Philpott, Principles of early drug discovery, *Br. J. Pharmacol.*, 2011, **162**, 1239–1249.
2 D. Sun, W. Gao, H. Hu and S. Zhou, Why 90% of clinical drug development fails and how to improve it?, *Acta Pharm. Sin. B*, 2022, **12**, 3049–3062.
3 T. C. Ezike, U. S. Okpala, U. L. Onoja, C. P. Nwike, E. C. Ezeako, O. J. Okpara, C. C. Okoroafor, S. C. Eze, O. L. Kalu, E. C. Odoh, U. G. Nwadike, J. O. Ogbodo, B. U. Umeh, E. C. Ossai and B. C. Nwanguma, Advances in Drug Delivery Systems, Challenges and Future Directions, *Heliyon*, 2023, **9**, e17488.
4 P. Hassanzadeh, F. Atyabi and R. Dinarvand, Technical and engineering considerations for designing therapeutics and delivery systems, *J. Controlled Release*, 2023, **353**, 411–422.
5 P. Davoodi, L. Y. Lee, Q. Xu, V. Sunil, Y. Sun, S. Soh and C. H. Wang, Drug delivery systems for programmed and on-demand release, *Adv. Drug Delivery Rev.*, 2018, **132**, 104–138.
6 P. Wei, E. J. Cornel and J. Du, Ultrasound-responsive polymer-based drug delivery systems, *Drug Delivery Transl. Res.*, 2021, **11**, 1323–1339.
7 R. Gannimani, P. Walvekar, V. R. Naidu, T. M. Aminabhavi and T. Govender, Acetal containing polymers as pH-responsive nano-drug delivery systems, *J. Controlled Release*, 2020, **328**, 736–761.
8 M. Shahriari, M. Zahiri, K. Abnous, S. M. Taghdisi, M. Ramezani and M. Alibolandi, Enzyme responsive drug delivery systems in cancer treatment, *J. Controlled Release*, 2019, **308**, 172–189.
9 S. Hossen, M. K. Hossain, M. K. Basher, M. N. H. Mia, M. T. Rahman and M. J. Uddin, Smart nanocarrier-based drug delivery systems for cancer therapy and toxicity studies: a review, *J. Adv. Res.*, 2019, **15**, 1–18.
10 J. Majumder, O. Taratula and T. Minko, Nanocarrier-based systems for targeted and site specific therapeutic delivery, *Adv. Drug Delivery Rev.*, 2019, **144**, 57–77.
11 S. Z. Alshawwa, A. A. Kassem, R. M. Farid, S. K. Mostafa and G. S. Labib, Nanocarrier drug delivery systems: characterization, limitations, future perspectives and implementation of artificial intelligence, *Pharmaceutics*, 2022, **14**, 883.
12 V. Almeida-Marrero, F. Bethlehem, S. Longo, M. C. Bertolino, T. Torres, J. Huskens and A. de la Escosura, Tailored multivalent targeting of siglecs with photosensitizing liposome nanocarriers, *Angew. Chem., Int. Ed.*, 2022, **61**, e202206900.
13 S. Karamchedu, L. Tunki, H. Kulhari and D. Pooja, Morin hydrate loaded solid lipid nanoparticles: characterization, stability, anticancer activity, and bioavailability, *Chem. Phys. Lipids*, 2020, **233**, 104988.
14 X. Xie, Y. Kurashina, M. Matsui, T. Nomoto, M. Itoh, H. J. Okano, K. Nakamura, N. Nishiyama and Y. Kitamoto, Transdermal delivery of bFGF with sonophoresis facilitated by chitosan nanocarriers, *J. Drug Delivery Sci. Technol.*, 2022, **75**, 103675.
15 D. Pooja, T. S. Reddy, H. Kulhari, A. Kadari, D. J. Adams, V. Bansal and R. Sistla, N-Acetyl-d-glucosamine-conjugated PAMAM dendrimers as dual receptor-targeting nanocarriers for anticancer drug delivery, *Eur. J. Pharm. Biopharm.*, 2020, **154**, 377–386.
16 S. C. Burkert, X. Y. He, G. V. Shurin, Y. Nefedova, V. E. Kagan, M. R. Shurin and A. Star, Nitrogen-doped carbon nanotube cups for cancer therapy, *ACS Appl. Nano Mater.*, 2022, **5**, 13685–13696.
17 M. A. Gonzalez-Lopez, E. M. Gutierrez-Cardenas, C. Sanchez-Cruz, J. F. Hernandez-Paz, I. Perez, J. J. Olivares-Trejo and O. Hernandez-Gonzalez, Reducing the effective dose of cisplatin using gold nanoparticles as carriers, *Cancer Nano*, 2020, **11**, 4.
18 L. Wang, N. Wang, W. Zhang, X. Cheng, Z. Yan, G. Shao, X. Wang, R. Wang and C. Fu, Therapeutic peptides: current applications and future directions, *Signal Transduction Targeted Ther.*, 2022, **7**, 48.
19 A. Levin, T. A. Hakala, L. Schnaider, G. J. L. Bernardes, E. Gazit and T. P. J. Knowles, Biomimetic peptide self-assembly for functional materials, *Nat. Rev. Chem.*, 2020, **4**, 615–634.
20 W. Y. Li, F. Separovic, N. M. O'Brien-Simpson and J. D. Wade, Chemically modified and conjugated antimicrobial peptides against superbugs, *Chem. Soc. Rev.*, 2021, **50**, 4932–4973.
21 V. B. Kumar, B. Ozguney, A. Vlachou, Y. Chen, E. Gazit and P. Tamamis, Peptide self-assembled nanocarriers for cancer drug delivery, *J. Phys. Chem. B*, 2023, **127**, 1857–1871.
22 D. Berillo, A. Yeskendir, Z. Zharkinbekov, K. Raziyeva and A. Saparov, Peptide-based drug delivery systems, *Medicina*, 2021, **57**, 1209.
23 S. Tarvirdipour, M. Skowicki, V. Maffeis, S. N. Abdollahi, C.-A. Schoenenberger and C. G. Palivan, Peptide nanocarriers co-delivering an antisense oligonucleotide and photosensitizer elicit synergistic cytotoxicity, *J. Colloid Interface Sci.*, 2024, **664**, 338–348.
24 Z. Y. Gong, B. L. Zhou, X. Y. Liu, J. J. Cao, Z. X. Hong, J. Y. Wang, X. R. Sun, X. M. Yuan, H. N. Tan, H. J. Ji and J. K. Bai, Enzyme-induced transformable peptide nanocarriers with enhanced drug permeability and retention to improve tumor nanotherapy efficacy, *ACS Appl. Mater. Interfaces*, 2021, **13**, 55913–55927.
25 S.-J. Mun, E. Cho, J.-S. Kim and C.-S. Yang, Pathogen-derived peptides in drug targeting and its therapeutic approach, *J. Controlled Release*, 2022, **350**, 716–733.
26 D. N. Woolfson, A brief history of de novo protein design: minimal, rational, and computational, *J. Mol. Biol.*, 2021, **433**, 167160.

27 D. N. Woolfson, The design of coiled-coil structures and assemblies, *Adv. Protein Chem.*, 2005, **70**, 79–112.
28 D. N. Woolfson, The physics, chemistry, and biology of α-helical coiled coils, *J. Biol. Chem.*, 2023, **299**, 104579.
29 W. M. Dawson, F. J. O. Martin, G. G. Rhys, K. L. Shelley, R. L. Brady and D. N. Woolfson, Coiled coils 9-to-5: rational de novo design of α-helical barrels with tunable oligomeric states, *Chem. Sci.*, 2021, **12**, 6923–6928.
30 M. R. Hicks, J. Walshaw and D. N. Woolfson, Investigating the tolerance of coiled-coil peptides to nonheptad sequence inserts, *J. Struct. Biol.*, 2002, **137**, 73–81.
31 J. L. Price, W. S. Horne and S. H. Gellman, Structural consequences of β-amino acid preorganization in a self-assembling α/β-peptide: fundamental studies of foldameric helix bundles, *J. Am. Chem. Soc.*, 2010, **132**, 12378–12387.
32 M. Szefczyk, N. Szulc, M. Gasior-Glogowska, A. Modrak-Wojcik, A. Bzowska, W. Majstrzyk, M. Taube, M. Kozak, T. Gotszalk, E. Rudzinska-Szostak and L. Berlicki, hierarchical approach for the rational construction of helix-containing nanofibrils using α,β-peptides, *Nanoscale*, 2021, **13**, 4000–4015.
33 M. Szefczyk, N. Szulc, M. Gasior-Glogowska, D. Bystranowska, A. Zak, A. Sikora, O. Polanska, A. Ozyhar and L. Berlicki, The application of the hierarchical approach for the construction of foldameric peptide self-assembled nanostructures, *Soft Matter.*, 2023, **19**, 3828–3840.
34 M. Szefczyk, K. Ozga, M. Drewniak-Switalska, E. Rudzinska-Szostak, R. Holubowicz, A. Ozyhar and L. Berlicki, Controlling the conformational stability of coiled-coil peptides with a single stereogenic center of a peripheral β-amino acid residue, *RSC Adv.*, 2022, **12**, 4640–4647.
35 D. Seebach, A. K. Beck and D. J. Bierbaum, The world of beta- and gamma-peptides comprised of homologated proteinogenic amino acids and other components, *Chem. Biodivers.*, 2024, **1**, 1111–1239.
36 P. Sang and J. Cai, Unnatural helical peptidic foldamers as protein segment mimics, *Chem. Soc. Rev.*, 2023, **52**, 4843–4877.
37 F. Clerici, E. Erba, M. L. Gelmi and S. Pellegrino, Non-standard amino acids and peptides: From self-assembly to nanomaterials, *Tetrahedron Lett.*, 2016, **57**, 5540–5550.
38 M. Szefczyk, Peptide foldamer-based self-assembled nanostructures containing cyclic beta-amino acids, *Nanoscale*, 2021, **13**, 11325–11333.
39 M. J. Sis and M. J. Webber, Drug delivery with designed peptide assemblies, *Trends Pharmacol. Sci.*, 2019, **40**, 747–762.
40 B. Yang, T. Wang, Y. Yang, H. Zhu and J. Li, The Application Progress of Peptides in Drug Delivery Systems in the Past Decade, *J. Drug Delivery Sci. Technol.*, 2021, **66**, 102880.
41 S. Eskandari, T. Guerin, I. Toth and R. J. Stephenson, Recent advances in self-assembled peptides: implications for targeted drug delivery and vaccine engineering, *Adv. Drug Delivery Rev.*, 2017, **110–111**, 169–187.
42 N. Habibi, N. Kamaly, A. Memic and H. Shafiee, Self-assembled peptide-based nanostructures: smart nanomaterials toward targeted drug delivery, *Nano Today*, 2016, **11**, 41–60.
43 J. Yang, H.-W. An and H. Wang, Self-assembled peptide drug delivery systems, *ACS Appl. Bio Mater.*, 2021, **4**, 24–46.
44 F. Thomas, W. M. Dawson, E. J. M. Lang, A. J. Burton, G. J. Bartlett, G. G. Rhys, A. J. Mulholland and D. N. Woolfson, De novo-designed α-helical barrels as receptors for small molecules, *ACS Synth. Biol.*, 2018, **7**, 1808–1816.
45 M. Nambiar, M. Nepal and J. Chmielewski, Self-assembling coiled-coil peptide nanotubes with biomolecular cargo encapsulation, *ACS Biomater. Sci. Eng.*, 2019, **5**, 5082–5087.
46 T. M. Laue, B. Shah, T. M. Ridgeway and S. L. Pelletier, in Computer-aided interpretation of analytical sedimentation data for proteins, ed. S. E. Harding, J. C. Hortong, A. J. Rowe, *Analytical ultracentrifugation in biochemistry and polymer science*, Royal Society of Chemistry, Cambridge, UK, 1992, pp. 90–125.
47 H. Durchschlag and P. Zipper, Calculation of partial specific volumes and other volumetric properties of small molecules and polymers, *J. Appl. Crystallogr.*, 1997, **30**, 803–807.
48 H. Zhao, R. Ghirlando, G. Piszczek, U. Curth, C. A. Brautigam and P. Schuck, Recorded scan times can limit the accuracy of sedimentation coefficients in analytical ultracentrifugation, *Anal. Biochem.*, 2013, **437**, 104–108.
49 P. Schuck, Sedimentation analysis of noninteracting and self-associating solutes using numerical solutions to the Lamm equation, *Biophys. J.*, 1998, **75**, 1503–1512.
50 P. Schuck, Size-distribution analysis of macromolecules by sedimentation velocity ultracentrifugation and Lamm equation modeling, *Biophys. J.*, 2000, **78**, 1606–1619.
51 J. Walshaw and D. N. Woolfson, Extended knobs-into-holes packing in classical and complex coiled-coil assemblies, *J. Struct. Biol.*, 2003, **144**, 349–361.
52 G. G. Rhys, W. M. Dawson, J. L. Beesley, F. J. O. Martin, R. L. Brady, A. R. Thomson and D. N. Woolfson, How coiled-coil assemblies accommodate multiple aromatic residues, *Biomacromolecules*, 2021, **22**, 2010–2019.
53 K. I. Albanese, R. Petrenas, F. Pirro, E. A. Naudin, U. Borucu, W. M. Dawson, D. A. Scott, G. J. Leggett, O. D. Weiner, T. A. A. Oliver and D. N. Woolfson, Rationally seeded computational protein design of α-helical barrels, *Nat. Chem. Biol.*, 2024, **20**, 991–999.
54 M. Oba, C. Ito and M. Tanaka, Effects of five-membered ring amino acid incorporation into peptides for coiled coil formation, *Bioorg. Med. Chem. Lett.*, 2018, **28**, 875–877.
55 D. Balandin, N. Szulc, D. Bystranowska, M. Gąsior-Głogowska, R. Kruszakin and M. Szefczyk, Boosting stability: a hierarchical approach for self-assembling peptide structures, *J. Mater. Chem. B*, 2024, **12**, 10682–10691.
56 M. Szefczyk, J. Lizandra Perez, A. Szczepanska and P. Fortuna, In *Alternative carriers in drug delivery systems – peptide foldamers*, *Proceedings of the 8th World Congress on Recent Advances in Nanotechnology (RAN'23)*, Lisbon, Portugal – March 23–25, 2023, Paper No. ICNNFC 109.
57 J. Lopez-Llano, L. A. Campos and J. Sancho, Alpha-helix stabilization by alanine relative to glycine: Roles of polar and apolar solvent exposures and of backbone entropy, *Proteins*, 2006, **64**, 769–778.
58 L. Serrano, J. L. Neira, J. Sancho and A. R. Fersht, Effect of alanine versus glycine in alpha-helices on protein stability, *Nature*, 1992, **356**, 453–455.